Organic compounds from macroalgal emission dominate new particle growth initiated by iodine species in coastal atmosphere

Yibei Wan[1], Xiangpeng Huang[2], Chong Xing[1], Qiongqiong Wang[1], Xinlei Ge[2], Huan Yu[1,*]

[1] School of Environmental Studies, China University of Geosciences, Wuhan, 430074, China

[2] Jiangsu Key Laboratory of Atmospheric Environment Monitoring and Pollution Control, Collaborative Innovation Center of Atmospheric Environment and Equipment Technology, School of Environmental Science and Engineering, Nanjing University of Information Science and Technology, Nanjing 210044, China

* To whom correspondence should be addressed: yuhuan@cug.edu.cn

Abstract

Iodine-initiated new particle formation (I-NPF) has long been recognized in coastal hotspot regions. However, no prior work has studied the exact chemical composition of organic compounds and their role in the coastal I-NPF. Here we present an important complementary study to the ongoing laboratory and field researches of iodine nucleation in coastal atmosphere. Oxidation and NPF experiments with vapor emissions from real-world coastal macroalgae were simulated in a bag reactor. On the basis of comprehensive mass spectrometry measurements, we reported for the first time a series of volatile precursors and their oxidation products in gas and particle phases in such a highly complex system. Organic compounds overwhelmingly dominated over iodine in the new particle growth initiated by iodine species. This study provided a more complete story of coastal NPF from low-tide macroalgal emission.

1. Introduction

Coastal new particle formation (NPF) may be driven by daytime low-tide emission of iodine species from macroalgae fully or partially exposed to the air. The phenomenon was reported in hotspot locations of west Europe, Australia and polar regions [*Allan et al., 2015; Baccarini et al., 2020; Beck et al., 2021; Heard et al., 2006; McFiggans et al., 2010; O'Dowd et al., 2002; Sipilä et al., 2016; Whitehead et al., 2009*]. In the southeast coastline of China, we reported intense iodine-initiated NPF based on particle number size distribution and iodine measurements [*Yu et al., 2019*].

To simulate iodine-initiated NPF (I-NPF) in controlled laboratory conditions, I_2 or CH_2I_2 vapor

was usually photolyzed in the presence of ozone to provide nucleation precursor [*Burkholder et al., 2004; He et al., 2021; Huang et al., 2022; Jimenez et al., 2003; Martín et al., 2020; Monahan et al., 2012; O'Dowd et al., 2004; Saunders and Plane, 2005*]. *Ashu-Ayem et al.* [*2012*]; *McFiggans et al.* [*2004*]; *Monahan et al.* [*2012*]; *Sellegri et al.* [*2005*] and *Sellegri et al.* [*2016*] also investigated the NPF from the vapors emitted by real-world macroalgal specimens or seawater in laboratory chamber or apparatus. However, the focus of all above studies are emission rate, oxidation mechanisms or nucleation pathways of iodine species. For example, positive correlations between particle concentrations and I_2 or CH_2I_2 mixing ratios were usually observed [*Burkholder et al., 2004; Jimenez et al., 2003; Monahan et al., 2012; Sellegri et al., 2005*]. Kinetic studies in flow tube or CERN CLOUD chamber proposed the clustering of iodine oxides (I_xO_y) or iodine oxoacids (HIO_3, HIO_2) as nucleation mechanisms on the basis of photoionization TOF-MS [*Martín et al., 2020*], Api-TOF and nitrate-Chemical Ionization Mass Spectrometer (CIMS) measurements [*He et al., 2021*]. A recent chamber study showed heterogeneous reaction between iodine oxide nanoparticle, meso-erythritol (or glyoxal) and dimethylamine accelerated nanoparticle growth [*Huang et al., 2022*].

Until now, no prior work has investigated the exact chemical identity of organic compounds (other than iodinated methane) and their role in I-NPF. The role of biogenic terpenes and anthropogenic aromatics in continental NPF has been recognized for a long time [*Donahue et al., 2013*]. Their ozonolysis or photochemistry products have been investigated in depth by using Electrospray Ionization Mass Spectrometry (ESI-MS) and more recently CIMS [*Ehn et al., 2014; Faxon et al., 2018; Kundu et al., 2012; Kundu et al., 2017; Nguyen et al., 2010; Riva et al., 2017; Wang et al., 2020; Yan et al., 2020*]. It is very likely that certain volatile organic compounds (VOCs) emitted mutually with iodine or iodinated methane from coastal biota or biologically active sea surface may also be involved in coastal I-NPF process and promote the growth of iodine particles.

To test this hypothesis, we conducted oxidation and NPF experiments with vapor emissions from real-world coastal macroalgae in a bag reactor. A suite of mass spectrometric methods including Inductively Coupled Plasma-MS (ICP-MS), Gas Chromatography-MS (GC-MS), ESI-orbitrap MS and iodide-CIMS were applied to measure vapor precursors, gaseous products and particulate products during the NPF process. Mass concentrations of total organic carbon (TOC) and total iodine (TI) of new particles were compared to evaluate the relative importance of organics and iodine in new particle growth. The identity and transformation mechanisms of organic compounds were identified to provide a more complete story of coastal NPF from low-tide macroalgal emission. Our study is thus complementary to prior laboratory and field studies of I-NPF, but has an emphasis on organics.

2. Experiments

2.1 Experimental apparatus and sample collection

Similar to Potential Aerosol Mass (PAM) Oxidation Flow Reactor, a bag reactor was designed to provide an oxidizing environment for simulating atmospheric oxidation processes of algae-emitted VOCs. The bag reactor was made from 75 µm-thick fluorinated ethylene propylene (FEP) Teflon (1.2 m×1.5 m, flat dimension). The volume of the bag at full inflation was determined experimentally to be about 200 L. The bag was suspended vertically (Figure S1) and kept in the dark or directly exposed to room light of fluorescent lamp. Because the purpose of this study is to qualitatively measure the oxidation products of algae-emitted VOCs, wall loss, production rate and other kinetic factors in the bag reactor were not evaluated. Fresh macroalgae (*Undaria pinnatifida*) was collected from intertidal zone at Xiangshan gulf of east China coast and stored at -10 $^\circ$C until the experiments. 2 kg macroalgae was put in a 20 L Pyrex glass bottle that was filled with ~1 L natural seawater. The specimens was partially exposed to the air to simulate tidal emersion of macroalgae. A flow of particle-free ultra high purity (UHP) air blew the algae-emitted VOCs out of the bottle and merged with a diluting air flow before entering the bag reactor.

Two types of experiments were conducted. In the three ozonolysis experiments, ozone (O_3) was generated by flowing an UHP air flow through a 5 Watts 185 nm UV lamp. The O_3 flow was fed just before the bag reactor was fully inflated. Final O_3 concentration in the bag reactor was measured to be ~200 ppbv using an ozone analyzer (Model 49i, Thermo-Fisher Scientific Inc.). In an additional OH-enhanced experiment, the O_3/VOC mixture flow was directed through a 254 nm UV light before entering the bag reactor. OH radicals were produced via the reaction $O_3 + h\nu \rightarrow O_2 + O(^1D)$ and $O(^1D) + H_2O \rightarrow 2OH$.

Before each experiment, the bag was purged for several hours to reduce background particle concentrations to below 1 cm^{-3}. The bag reactor was first operated in a static mode to monitor the time evolution of gaseous products and particle size, and then in a dynamic mode to collect enough particles for offline chemical analysis. In the static mode, the bag was first filled to full inflation with the VOCs/O_3 flows. The flows were then shut down; a Scanning Mobility Particle Sizer (SMPS, model 3936, TSI Inc., Shoreview, MN, USA) and an Aerodyne iodide-CIMS pulled two flows of 0.3 liters per minute (lpm) and 1.8 lpm out of the bag, respectively. The SMPS measured the particle number size distribution from 14 to 600 nm.

In the dynamic mode, the VOCs/O_3 flow of 3 lpm was fed to the bag continuously, while the

96 SMPS and a vacuum pump (GAST Group Ltd.) pulled sample flows of 0.3 and 2.7 lpm, respectively,

97 out of the bag reactor. This resulted in an overall residential time of 67 minutes for the O_3/VOC

98 mixture in the fully inflated bag. The particles in the 2.7 lpm sample flow were collected onto a

99 Zefluor® PTFE membrane filter mounted in a filter inlet for gases and aerosols (FIGAERO) for

100 iodide-CIMS analysis, or alternatively, onto 47 mm diameter double quartz fiber filter pack mounted

101 in a filter holder for ESI-orbitrap MS, ICP-MS and TOC analysis. The front filter of the double filter

102 pack collected the particles, while the back filter placed downstream of the front filter was supposed

103 to adsorb the same amount of volatile species as the front filter.

104 **2.2 Chemical analysis**

105   Before the ozonolysis experiments, the algae-emitted VOCs in the bag reactor was collected by a

106 6-liter pre-evacuated stainless-steel canisters (Entech Instruments, Inc., Simi Valley, CA, USA) and

107 was analyzed using a quadrupole GC-MS system (model TH-300B, Wuhan Tianhong Instruments Co.

108 Ltd., Wuhan, China). The algae-emitted VOCs, as well as their gaseous and particulate products,

109 were also measured by the FIGAERO-iodide-CIMS. Iodide-adduct chemical ionization is well suited

110 for measuring oxygenated or acidic compounds with minimal fragmentation. More details of the

111 GC-MS and FIGAERO-iodide-CIMS measurements can be found in Supporting Material. The

112 theory and design of the two instruments were described by *Wang et al.* [*2014*] and *Lopez-Hilfiker et*

113 *al.* [*2014*].

114   The particles collected on quartz fiber filters were sent for offline quantification of TOC and TI,

115 as well as non-target analysis of organic compounds using ESI-orbitrap MS. The front and back

116 filters were treated, separately, following the procedure as below: the filter was ultrasonicated twice

117 with 10-mL water and acetone nitrile solvent mixture (v:v=1:1). The extract was filtered by a 0.2 μm

118 PTFE syringe filter and evaporated in a rotary evaporator to 0.5 mL. After being centrifuged for 30

119 min at 12000 rpm, the supernatant was collected for TI analysis by Agilent 1100 HPLC-7900

120 ICP-MS (Agilent Technologies, Santa Clara, CA, USA) and TOC analysis by a TOC analyzer

121 (Model TOC-5000A, Shimadzu, Japan). TI or TOC in the particles was obtained by subtracting the

122 amount on the back filter from that on the front filter. Nontarget analysis of organic compounds in

123 the supernatant was conducted using a Q Exactive hybrid Quadrupole-Orbitrap mass spectrometer

124 (Thermo Scientific, Bremen, Germany). The supernatant was directly infused by a syringe pump and

125 ionized in negative ESI source. All the ions in the m/z range from 50 to 500 Th were scanned with a

126 mass resolution of 70000. The chemically sound CHO molecular formulas were computed with a

127 mass tolerance of ±2 ppm for these ions. Only the compounds that existed solely in the front filter or

128 with ion intensity in the front filter higher than that in the back filter by a factor of 3 were regarded

129 as the organic compounds in the particle phase.

130 **3. Results and discussion**

131 **3.1 Relative mass contribution of organic carbon and iodine to new particles**

132 Typical banana-shape particle size spectrum observed in the static mode of an ozonolysis

133 experiment is shown in Figure 1a. In the presence of room light, new particles larger than 14 nm

134 were observed only 58 minutes after the injection of ozone flow. This relative long time is due to the

135 build-up of O_3 concentration and subsequent accumulation of oxidation products. No particles were

136 formed in the absence of room light or ozone. In the dynamic mode experiments, O_3 in the bag

137 reactor was kept at its maximum concentration 200 ppbv. With a prolonged residential time of 67

138 min, the particles grew to 102±23 nm, which was measured by the SMPS at the outlet of the bag

139 reactor. The TOC and TI measurements show that organic compounds contributed more particle

140 mass than iodine with TOC/(I+TOC) ratio of 96.1±2.9% (Table 1).

141 In the OH-enhanced experiment (dynamic mode), more particulate products were generated with

142 enhanced oxidation capacity: TI in the particles increased by a factor of 10.8; TOC increased by a

143 factor of 2.7; particle number concentration increased by a factor of 7.4. On the other hand, particle

144 size decreased to 73 nm and TOC/(TI+TOC) ratio decreased to 92.9% (Table 1). These differences

145 indicate that more iodine nuclei were produced with enhanced OH concentration, probably via

146 OIO+OH$\rightarrow$ HOIO$_2$ [*Plane et al., 2006*]. Competitive uptake of condensing organic vapors onto these

147 iodine nuclei limited the growth of individual new particles. Nevertheless, organic compounds

148 overwhelmingly dominated over iodine in the mass contribution to new particle growth.

149 The significant organic contribution observed in the laboratory condition is generally consistent

150 with TOC/(I+TOC) ratio of 98.2% in 10-56 nm new particles collected during a coastal I-NPF event in

151 China [*Yu et al., 2019*], although TOC and TI during the field event are two orders of magnitude

152 lower than those in the bag reactor (Table 1). Mean diameter of new particles was observed to be

153 only 16 nm during the field event. But those small new particles are expected to grow into CCN

154 active sizes, given longer residence time and uptake of more condensing vapors in the atmosphere.

155 **3.2 Macroalgal emission**

156 It is of particular interest to know what VOCs are emitted from coastal macroalgae. They are

157 potential precursors of iodine particle nucleation and growth. The canister sampling followed by

158 GC-MS analysis showed that the top 9 non-CHO compounds with highest TIC peak areas (Table 2)

159 are C_5 alkanes, C_{10} alpha-pinene and halogenated C_1, C_3 and C_5 alkanes. The top 10 CHO

160 compounds are C_2-C_6 alcohols and carbonyls with saturated or unsaturated carbon chain.

161 Iodide-CIMS is more sensitive to more oxygenated or acidic compounds and thus complementary

162 to the GC-MS measurement. The 76 organic precursors detected by iodide-CIMS before ozone

163 addition were characterized by $C_{1,2,3,6}$ and O_{2-3} formulas (Figure 2a). The top 7 compounds with

164 highest ion intensities were CH_2O_2, $C_2H_4O_2$, $C_3H_6O_3$, $C_6H_{10}O_3$, $C_2H_6O_2$, $C_4H_8O_2$ and $C_6H_{12}O_3$,

165 which accounted for 82.5% of total ion intensity. They are C_1-C_6 mono-carboxylic acids, hydroxyl

166 carboxylic acids or oxo-carboxylic acids with 2 to 3 oxygen atoms (Table 2). Their carbon atom

167 numbers are in general consistent with the VOCs detected by GC-MS.

168 Relatively high signals of HNO_3 were observed as NO_3^- and HNO_3I^- before the addition of ozone

169 to the bag reactor. Because HNO_3 and HNO_2 were also observed as deprotonated ions or I^- clusters in

170 the particle phase during the NPF, HNO_3 is also an important precursor of particle formation.

171 **3.3 Gaseous and particulate products**

172 **3.3.1 Inorganic molecules and radicals**

173 Being different from nitrate-CIMS, our iodide-CIMS did not detect nucleating clusters of iodine

174 oxides or oxyacids after the addition of ozone. Instead, dozens of new inorganic molecules or

175 radicals were observed as clusters with I^-, NO_3^- or deprotonated ions in the gas or particle phase

176 (Figure S2). We grouped these species by elemental composition and investigated their role in the

177 NPF by observing how their gaseous ion intensities evolved during the NPF event in the bag reactor

178 (Figure 1b-1e).

179 1. Cl, I, Cl_2 and ClI in the gas phase: the intensities of I and Cl increased ca. 10 minutes before 14

180 nm particles appeared and decreased as the particles grew up. Based on prior work of *Burkholder et*

181 *al.* [*2004*]; *Jimenez et al.* [*2003*]; *O'Dowd et al.* [*2004*], we suggested the photolysis of CH_2Cl_2,

182 CHBrCl, CH_3I and C_3H_7I was the source of halogen atoms (e.g., CH_3I+hv$\rightarrow$ CH_3+I). There was a

183 time lag of 20-25 minutes between the appearances of Cl and I and those of ClI and Cl_2, which were

184 probably from the recombination of Cl and I atoms.

185 2. IO_2, IO, ClIO, INO_2 and $ClNO_2$ in the gas phase: these species showed a similar time series to I

186 and Cl atoms. IO, IO_2 and ClIO could be from the reactions between I, ClI and O_3. INO_2 is usually

187 thought to form upon the reaction I+NO_2+M $\rightarrow INO_2$+M [*Saiz-Lopez et al., 2012*]. $ClNO_2$ was likely

188 to form upon similar reaction between Cl and NO_2 in the bag reactor.

189　　3. HIO_3 and INO_3: the two species seem to be the end products of above intermediates, because

190　　their intensities kept on increasing during new particle growth. INO_3, which is iodine nitrate $IONO_2$,

191　　was detected in both gas and particle phases. $IONO_2$ probably formed upon the recombination of IO

192　　and NO_2 ($IO+NO_2+M \rightarrow IONO_2+M$) [*Saiz-Lopez et al., 2012*]. HIO_3 was likely to form via

193　　$OIO+OH \rightarrow HOIO_2$ or $I + H_2O + O_3 \rightarrow HOIO_2 + OH$ [*Martín et al., 2020; Plane et al., 2006*]. HIO_3

194　　was not detected in particle phase by iodide-CIMS, which is contrary to the observation by

195　　HPLC-ICP-MS that total iodine was mostly dominated IO_3^- peak. The signals of IO^-, IO_2^- and

196　　$HIONO_3^-$ in the particle phase are therefore most likely to result from thermal decomposition of

197　　HIO_3 to HIO and HIO_2 in the FIGAERO thermal desorption process.

198　　4. CH_3SO_3H, S_2^-, S_3^-, SO_3^-: We observed methane sulfonic acid (CH_3SO_3H, MSA) in both gas and

199　　particle phases. Gaseous MSA increased in the beginning, but decreased after new particles appeared

200　　(Figure 1f). Apparently, our measurement suggested MSA contributed to the growth of new particles,

201　　but it is unknown if it also participated in nucleation. We suggested S_2^-, S_3^-, SO_3^- ions observed in the

202　　particle phase were thermal decomposition products of MSA.

203　　**3.3.2 Gaseous organic products**

204　　After ozone addition, a gradual transformation from C_1-C_3 precursors to C_5-C_8 gaseous products

205　　was observed during the NPF process (Figure 1h). In the meanwhile, the oxygen atom number of the

206　　compounds increased from 2-3 to 4-7 (Figure 1g). The formation of compounds with more carbon

207　　atoms than the parent VOCs is unlikely in the gas phase, except bimolecular reactions of stabilized

208　　Criegee intermediates (SCIs) that typically form upon alkene ozonolysis. Similar to isoprene

209　　ozonolysis [*Inomata et al., 2014; Riva et al., 2017*], we propose the SCI addition mechanism can

210　　also explain the transformation observed in our case: (1) C_4 SCIs formed upon the ozonolysis of

211　　CHO precursors with C=C double bonds (e.g., those observed by GC-MS in Table 2). (2) the

212　　insertion of C_4 SCIs into carboxylic acid precursors (e.g., those observed by CIMS in Table 2)

213　　produced oligomeric hydroperoxides. An example was shown in Scheme I for the reactions of most

214　　abundant ethyl vinyl carbinol ($C_5H_{10}O$), ozone and formic acid (CH_2O_2), but the same mechanism is

215　　also applicable for ethyl vinyl ketone (C_5H_8O) and other abundant C_2-C_5 carboxylic acids and

216　　hydroxyl carboxylic acids. As a result, a series of gaseous oligomeric hydroperoxides $C_5H_{10}O_5$,

217　　$C_6H_{10}O_5$, $C_6H_{12}O_5$, $C_7H_{12}O_6$, $C_7H_{14}O_6$, $C_8H_{14}O_5$, $C_8H_{16}O_6$, $C_8H_{16}O_5$ and $C_9H_{16}O_6$ were observed with

218　　high intensity by iodide-CIMS.
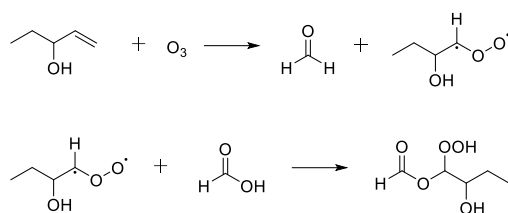
Scheme I

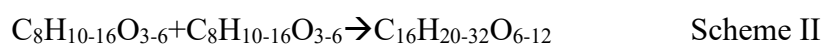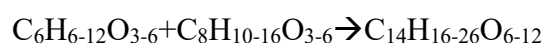### 3.3.3 Particulate organic products

In the end of a typical ozonolysis experiment (dynamic mode), 100 and 364 new formulas were observed in the gas and particle phases, respectively, including 73 semi-VOCs appeared in both gas and particle phases. Those semi-VOCs accounted for 81 and 20% of total ion intensities of gaseous and particulate products, respectively. Being different from unimodal atom number distributions of gaseous products (C_{max}= 7 and O_{max}=5, Figure 2b), particulate products were characterized by distinct bimodal or trimodal distribution of carbon number (C_{max}=8, 14 and 16, Figure 2c) and oxygen number (O_{max}=4 and 8), implying possible dimer formation via accretion reactions in the particle phase.

ESI-Orbitrap MS differs from FIGAERO-iodide-CIMS in extraction method (ultrasonic solvent extraction from quartz fiber filter *vs.* thermal desorption from PTFE membrane filter), ionization source (electrospray ionization *vs.* iodide-adduct chemical ionization) and MS resolving power (70000 *vs.* 4500). The result showed that ESI-orbitrap MS and FIGAERO-iodide-CIMS detected 336 and 364 organic formulas, respectively, in the particle phase. 167 organic formulas were commonly observed by both methods, which accounted for 87% and 54% of total ion intensity of organic formulas by the two methods, respectively (Figure S3). As shown in Figure 2c and 2d, FIGAERO-iodide-CIMS had better sensitivity toward the organic compounds with more oxygen atoms (e.g., O$\geq$8) and carbon atoms (e.g., C$\geq$10). As a result, bimodal carbon and oxygen atom number distributions were observed by FIGAERO-iodide-CIMS, but not ESI-orbitrap MS.

The measurement by ESI-orbitrap MS provided more insights about the formation mechanism of particulate products. We compared the 336 formulas detected by ESI-orbitrap MS in our study with the 414 formulas of isoprene ozonolysis SOA products [*Nguyen et al., 2010*] and 922 formulas of alpha-pinene ozonolysis SOA products [*Putman et al., 2012*] measured by the ESI-orbitrap MS. It was found that 72% of the formulas in this study can also be found in isoprene SOA, but only 39% can be found in alpha-pinene SOA. This seems to imply that some similar alkene ozonolysis reactions occurred in our system and isoprene ozonolysis.

For such a highly complex system full of various algae-emitted precursors, it is impossible to

247 simply propose a reaction mechanism to explain the formation of all particulate products, nor to list
248 all reactions occurring in the bag reactor. On the basis of particle-phase oligomer chemistry [*Seinfeld*
249 *and Pandis, 2016*], especially the well-understood isoprene ozonolysis SOA chemistry [*Inomata et*
250 *al., 2014; Nguyen et al., 2010; Riva et al., 2017*], we suggest a variety of accretion reactions without
251 uniform oligomerization pattern (e.g., esterification, aldol condensation, hemiacetal reactions,
252 peroxyhemiacetal formation and SCI reactions, etc.) transformed $O_{max}=4$ and $C_{max}=8$ multifunctional
253 monomers (like alcohols, carbonyls, hydroperoxides, carboxylic acids) to $O_{max}=8$ and $C_{max}=14$ or 16
254 dimers. Scheme II illustrated addition type self- and cross-oligomerization between C_6 and C_8
255 monomers produces C_{14} and C_{16} dimers. All the formulas in Scheme II are among the most abundant
256 ones observed in the particle phase by the iodide-CIMS.

257 $$C_6H_{6-12}O_{3-6}+C_8H_{10-16}O_{3-6}\rightarrow C_{14}H_{16-26}O_{6-12}$$

258 $$C_8H_{10-16}O_{3-6}+C_8H_{10-16}O_{3-6}\rightarrow C_{16}H_{20-32}O_{6-12}$$ Scheme II

259 **4. Conclusions**

260 Using a suite of mass spectrometers, we reported, for the first time, the chemical compositions of
261 volatile precursors emitted by real-world coastal macroalgae and their gaseous and particulate
262 oxidation products. In the presence of room light and ozone, the photolysis of halogenated $C_{1,3,5}$
263 alkanes ends up as HIO_3 and INO_3. It was most likely HIO_3 initiated NPF and provided nuclei for the
264 further condensation of other products like INO_3, MSA and CHO compounds. Gas-phase SCI
265 reactions and particle-phase accretion reactions transformed C_1-C_6 and O_2-O_3 precursors gradually to
266 particulate products with $C_{max}=8$, 14 and 16 and $O_{max}=4$ and 8. As a result, organic carbon were
267 found to overwhelmingly dominated over iodine in the mass contribution to the new particle growth.
268 Although our instruments did not allow the detection of nucleating clusters of iodine oxides or
269 oxyacids, our study provided important complementary information to the ongoing laboratory and
270 field researches of coastal I-NPF.

271 **Data Availability Statement**

272 All data related to figures and tables in this study are archived and made available through
273 Zenodo data repository https://doi.org/10.5281/zenodo.6965859.

References

Allan, J. D., et al. (2015), Iodine observed in new particle formation events in the Arctic atmosphere during ACCACIA, *Atmos. Chem. Phys.*, *15*(10), 5599-5609, doi:10.5194/acp-15-5599-2015.

Ashu-Ayem, E. R., U. Nitschke, C. Monahan, J. Chen, S. B. Darby, P. D. Smith, C. D. O'Dowd, D. B. Stengel, and D. S. Venables (2012), Coastal Iodine Emissions. 1. Release of I2 by Laminaria digitata in Chamber Experiments, *Environmental Science & Technology*, *46*(19), 10413-10421, doi:10.1021/es204534v.

Baccarini, A., et al. (2020), Frequent new particle formation over the high Arctic pack ice by enhanced iodine emissions, *Nature Communications*, *11*(1), 4924, doi:10.1038/s41467-020-18551-0.

Beck, L. J., et al. (2021), Differing Mechanisms of New Particle Formation at Two Arctic Sites, *Geophysical Research Letters*, *48*(4), e2020GL091334, doi:https://doi.org/10.1029/2020GL091334.

Burkholder, J. B., J. Curtius, A. R. Ravishankara, and E. R. Lovejoy (2004), Laboratory studies of the homogeneous nucleation of iodine oxides, *Atmospheric Chemistry and Physics*, *4*(1), 19-34, doi:10.5194/acp-4-19-2004.

Donahue, N. M., et al. (2013), How do organic vapors contribute to new-particle formation?, *Faraday Discussions*, *165*(0), 91-104, doi:10.1039/C3FD00046J.

Ehn, M., et al. (2014), A large source of low-volatility secondary organic aerosol, *Nature*, *506*(7489), 476-479, doi:10.1038/nature13032.

Faxon, C., J. Hammes, M. Le Breton, R. K. Pathak, and M. Hallquist (2018), Characterization of organic nitrate constituents of secondary organic aerosol (SOA) from nitrate-radical-initiated oxidation of limonene using high-resolution chemical ionization mass spectrometry, *Atmospheric Chemistry and Physics*, *18*(8), 5467-5481, doi:10.5194/acp-18-5467-2018.

He, X. C., et al. (2021), Role of iodine oxoacids in atmospheric aerosol nucleation, *Science*, *371*(6529), 589-595, doi:10.1126/science.abe0298.

Heard, D. E., et al. (2006), The North Atlantic Marine Boundary Layer Experiment(NAMBLEX). Overview of the campaign held at Mace Head, Ireland, in summer 2002, *Atmos. Chem. Phys.*, *6*(8), 2241-2272, doi:10.5194/acp-6-2241-2006.

Huang, R.-J., et al. (2022), Heterogeneous iodine-organic chemistry fast-tracks marine new particle formation, *Proceedings of the National Academy of Sciences*, *119*(32), e2201729119, doi:10.1073/pnas.2201729119.

Inomata, S., K. Sato, J. Hirokawa, Y. Sakamoto, H. Tanimoto, M. Okumura, S. Tohno, and T. Imamura (2014), Analysis of secondary organic aerosols from ozonolysis of isoprene by proton transfer reaction mass spectrometry, *Atmospheric Environment*, *97*, 397-405, doi:https://doi.org/10.1016/j.atmosenv.2014.03.045.

Jimenez, J. L., R. Bahreini, D. R. Cocker III, H. Zhuang, V. Varutbangkul, R. C. Flagan, J. H. Seinfeld, C. D. O'Dowd, and T. Hoffmann (2003), New particle formation from photooxidation of diiodomethane (CH2I2), *Journal of Geophysical Research: Atmospheres*, *108*(D10), doi:https://doi.org/10.1029/2002JD002452.

Kundu, S., R. Fisseha, A. L. Putman, T. A. Rahn, and L. R. Mazzoleni (2012), High molecular weight SOA formation during limonene ozonolysis: insights from ultrahigh-resolution FT-ICR mass spectrometry characterization, *Atmos. Chem. Phys.*, *12*(12), 5523-5536, doi:10.5194/acp-12-5523-2012.

Kundu, S., R. Fisseha, A. L. Putman, T. A. Rahn, and L. R. Mazzoleni (2017), Molecular formula composition of β-caryophyllene ozonolysis SOA formed in humid and dry conditions, *Atmospheric Environment*, *154*, 70-81, doi:https://doi.org/10.1016/j.atmosenv.2016.12.031.

Lopez-Hilfiker, F. D., et al. (2014), A novel method for online analysis of gas and particle composition: description and evaluation of a Filter Inlet for Gases and AEROsols (FIGAERO),

Atmospheric Measurement Techniques, 7(4), 983-1001, doi:10.5194/amt-7-983-2014.

Martín, J. C. G., T. R. Lewis, M. A. Blitz, J. M. C. Plane, M. Kumar, J. S. Francisco, and A. Saiz-Lopez (2020), A gas-to-particle conversion mechanism helps to explain atmospheric particle formation through clustering of iodine oxides, *Nature Communications*, 11(1), 4521, doi:10.1038/s41467-020-18252-8.

McFiggans, G., et al. (2010), Iodine-mediated coastal particle formation: an overview of the Reactive Halogens in the Marine Boundary Layer (RHaMBLe) Roscoff coastal study, *Atmospheric Chemistry and Physics*, 10(6), 2975-2999, doi:10.5194/acp-10-2975-2010.

McFiggans, G., et al. (2004), Direct evidence for coastal iodine particles from Laminaria macroalgae – linkage to emissions of molecular iodine, *Atmos. Chem. Phys.*, 4(3), 701-713, doi:10.5194/acp-4-701-2004.

Monahan, C., E. R. Ashu-Ayem, U. Nitschke, S. B. Darby, P. D. Smith, D. B. Stengel, D. S. Venables, and C. D. O'Dowd (2012), Coastal Iodine Emissions: Part 2. Chamber Experiments of Particle Formation from Laminaria digitata-Derived and Laboratory-Generated I2, *Environmental Science & Technology*, 46(19), 10422-10428, doi:10.1021/es3011805.

Nguyen, T. B., A. P. Bateman, D. L. Bones, S. A. Nizkorodov, J. Laskin, and A. Laskin (2010), High-resolution mass spectrometry analysis of secondary organic aerosol generated by ozonolysis of isoprene, *Atmospheric Environment*, 44(8), 1032-1042, doi:https://doi.org/10.1016/j.atmosenv.2009.12.019.

O'Dowd, C. D., J. L. Jimenez, R. Bahreini, R. C. Flagan, J. H. Seinfeld, K. Hämeri, L. Pirjola, M. Kulmala, S. G. Jennings, and T. Hoffmann (2002), Marine aerosol formation from biogenic iodine emissions, *Nature*, 417, 632, doi:10.1038/nature00775.

O'Dowd, C. D., M. C. Facchini, F. Cavalli, D. Cebrunis, M. Mircea, S. Decesari, S. Fuzzi, Y. J. Yoon, and J.-P. Putard (2004), Biogenically driven organic contribution to marine aerosol, *Nature*, 431, 676-680.

Plane, J. M. C., D. M. Joseph, B. J. Allan, S. H. Ashworth, and J. S. Francisco (2006), An Experimental and Theoretical Study of the Reactions OIO + NO and OIO + OH, *The Journal of Physical Chemistry A*, 110(1), 93-100, doi:10.1021/jp055364y.

Putman, A. L., J. H. Offenberg, R. Fisseha, S. Kundu, T. A. Rahn, and L. R. Mazzoleni (2012), Ultrahigh-resolution FT-ICR mass spectrometry characterization of α-pinene ozonolysis SOA, *Atmospheric Environment*, 46, 164-172, doi:https://doi.org/10.1016/j.atmosenv.2011.10.003.

Riva, M., S. H. Budisulistiorini, Z. F. Zhang, A. Gold, J. A. Thornton, B. J. Turpin, and J. D. Surratt (2017), Multiphase reactivity of gaseous hydroperoxide oligomers produced from isoprene ozonolysis in the presence of acidified aerosols, *Atmospheric Environment*, 152, 314-322, doi:10.1016/j.atmosenv.2016.12.040.

Saiz-Lopez, A., J. M. C. Plane, A. R. Baker, L. J. Carpenter, R. von Glasow, J. C. Gómez Martín, G. McFiggans, and R. W. Saunders (2012), Atmospheric Chemistry of Iodine, *Chemical Reviews*, 112(3), 1773-1804, doi:10.1021/cr200029u.

Saunders, R. W., and J. M. C. Plane (2005), Formation Pathways and Composition of Iodine Oxide Ultra-Fine Particles, *Environmental Chemistry*, 2(4), 299-303, doi:https://doi.org/10.1071/EN05079.

Seinfeld, J. H., and S. N. Pandis (2016), *Atmospheric chemistry and physics: from air pollution to climate change*, 3nd ed., John Wiley and Sons. Inc., New York.

Sellegri, K., et al. (2016), Evidence of atmospheric nanoparticle formation from emissions of marine microorganisms, *Geophysical Research Letters*, 43(12), 6596-6603, doi:https://doi.org/10.1002/2016GL069389.

Sellegri, K., Y. J. Yoon, S. G. Jennings, C. D. O'Dowd, L. Pirjola, S. Cautenet, H. Chen, and T. Hoffmann (2005), Quantification of Coastal New Ultra-Fine Particles Formation from In situ and Chamber Measurements during the BIOFLUX Campaign, *Environmental Chemistry*, 2(4), 260-270, doi:https://doi.org/10.1071/EN05074.
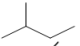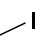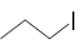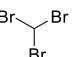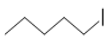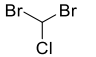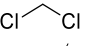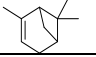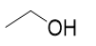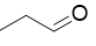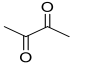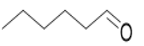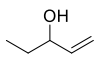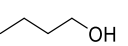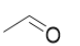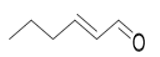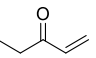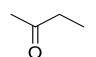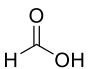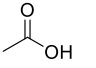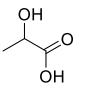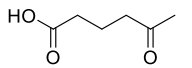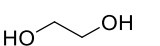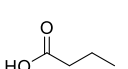
Sipilä, M., et al. (2016), Molecular-scale evidence of aerosol particle formation via sequential addition of HIO3, *Nature*, *advance online publication*, doi:10.1038/nature19314 http://www.nature.com/nature/journal/vaop/ncurrent/abs/nature19314.html#supplementary-information.

Wang, M., et al. (2020), Photo-oxidation of Aromatic Hydrocarbons Produces Low-Volatility Organic Compounds, *Environmental science & technology*, *54*(13), 7911-7921, doi:10.1021/acs.est.0c02100.

Wang, M., et al. (2014), Development and validation of a cryogen-free automatic gas chromatograph system (GC-MS/FID) for online measurements of volatile organic compounds, *Analytical Methods*, *6*(23), 9424-9434, doi:10.1039/C4AY01855A.

Whitehead, J. D., G. B. McFiggans, M. W. Gallagher, and M. J. Flynn (2009), Direct linkage between tidally driven coastal ozone deposition fluxes, particle emission fluxes, and subsequent CCN formation, *Geophysical Research Letters*, *36*(4), doi:doi:10.1029/2008GL035969.

Yan, C., et al. (2020), Size-dependent influence of NO(x) on the growth rates of organic aerosol particles, *Science advances*, *6*(22), eaay4945, doi:10.1126/sciadv.aay4945.

Yu, H., L. Ren, X. Huang, M. Xie, J. He, and H. Xiao (2019), Iodine speciation and size distribution in ambient aerosols at a coastal new particle formation hotspot in China, *Atmospheric Chemistry and Physics*, *19*(6), 4025-4039, doi:10.5194/acp-19-4025-2019.

Table 1. Particle number concentration (N), mean diameter (D_p), total organic carbon (TOC) and total iodine (TI) of new particles with a residential time of 67 min in the bag reactor in the ozonolysis experiments and OH-enhanced experiment (dynamic mode). Those of 10-56 nm new particles collected by a nano Micro-Orifice Uniform Deposit Impactor (nano-MOUDI, MSP, Inc.) during an I-NPF event at a coastal site of Ningbo, China (Yu *et al.*, 2019) were also listed.

	TOC (μg m^{-3})	TI (μg m^{-3})	TOC/(TI+TOC)	N (cm^{-3})	D_p (nm)
ozonolysis experiments	45.6±9.7	0.88±0.34	96.1±2.9%	(5.58±2.04)×10^4	102±23
OH-enhanced experiment	125.3	9.5	92.9%	4.16×10^5	73
I-NPF event at a coastal site of China	0.7	0.0135	98.2%	6.00×10^5	16

Table 2. Major volatile organic compounds emitted by macroalgae as potential NPF precursors, sorted by TIC peak area measured by GC/MS or MS peak intensity measured by iodide-CIMS

|	Formula	Structure	Peak area/MS peak intensity
1	C_5H_{12}		1.90×10^6
2	C_5H_{10}		1.59×10^6
3	CH_3I		1.37×10^6
4	C_3H_7I		7.60×10^5
5	$CHBr_3$		4.71×10^5
6	$C_5H_{11}I$		3.75×10^5
7	$CHBr_2Cl$		2.71×10^5
8	CH_2Cl_2		2.55×10^5
9	$C_{10}H_{16}$		2.26×10^5
1	C_2H_6O		1.70×10^7
2	C_3H_6O		1.38×10^7
3	$C_4H_6O_2$		1.30×10^7
4	$C_6H_{12}O$		1.03×10^7
5	$C_5H_{10}O$		1.00×10^7
6	$C_4H_{10}O$		5.16×10^7
8	C_2H_4O		3.46×10^7
9	$C_6H_{10}O$		2.88×10^7
7	C_5H_8O		1.45×10^7
10	C_4H_8O		1.37×10^7
1	CH_2O_2		1.58×10^6
2	$C_2H_4O_2$		9.52×10^5
3	$C_3H_6O_3$		9.21×10^5
4	$C_6H_{10}O_3$		4.44×10^5
5	$C_2H_6O_2$		2.88×10^5
6	$C_4H_8O_2$		1.17×10^5
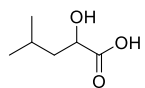
7    $C_6H_{12}O_3$ 1.12×10^5
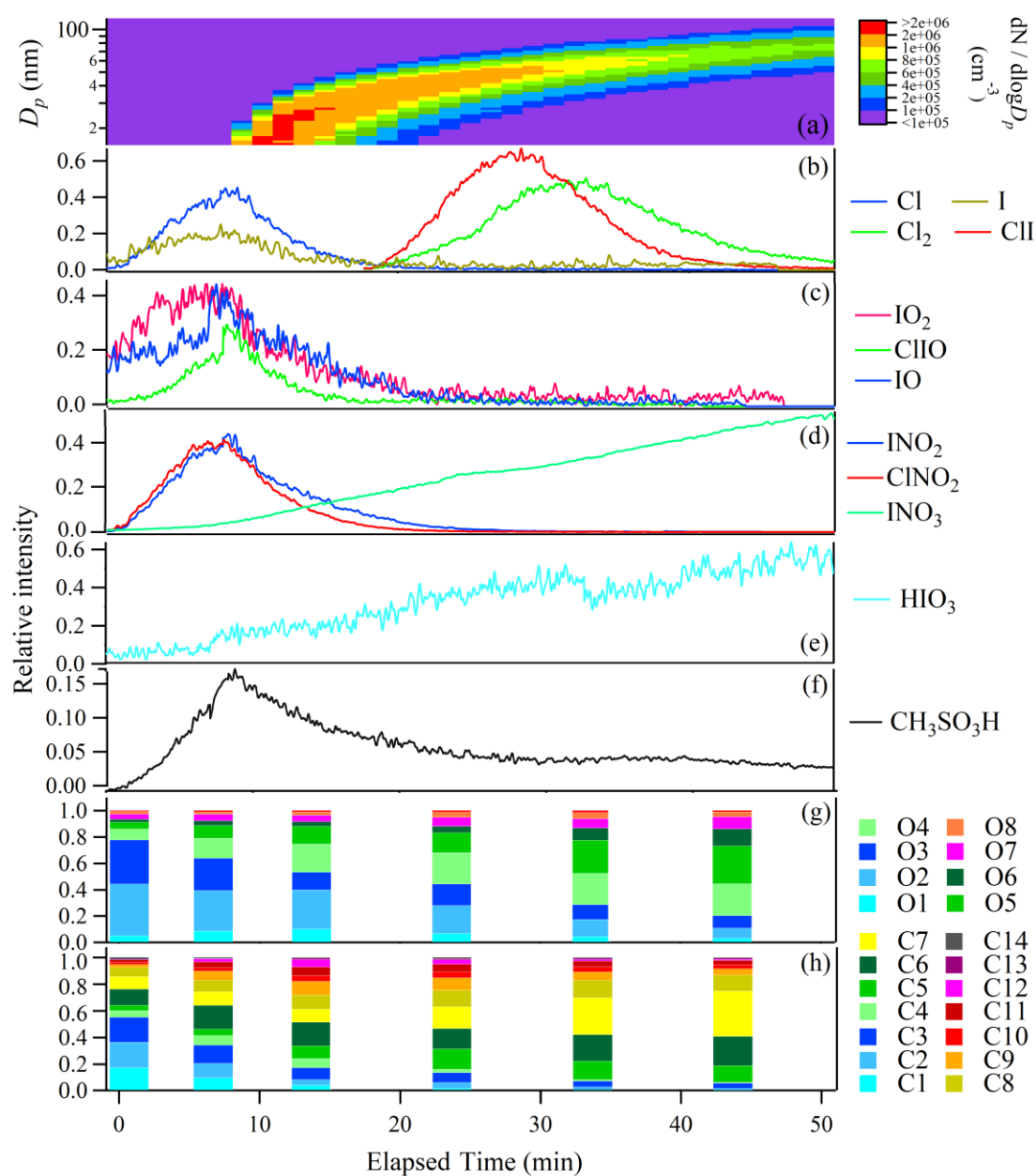
Figure 1. Time evolution of particle number size distribution (a) and relative intensities of gaseous molecules and radicals (b-f); the fractions of organic compounds grouped by O and C atom numbers in the selected time points (g-h) in a typical ozonolysis experiment (static mode). Time zero was chosen as the start time when HIO_3 was observed.
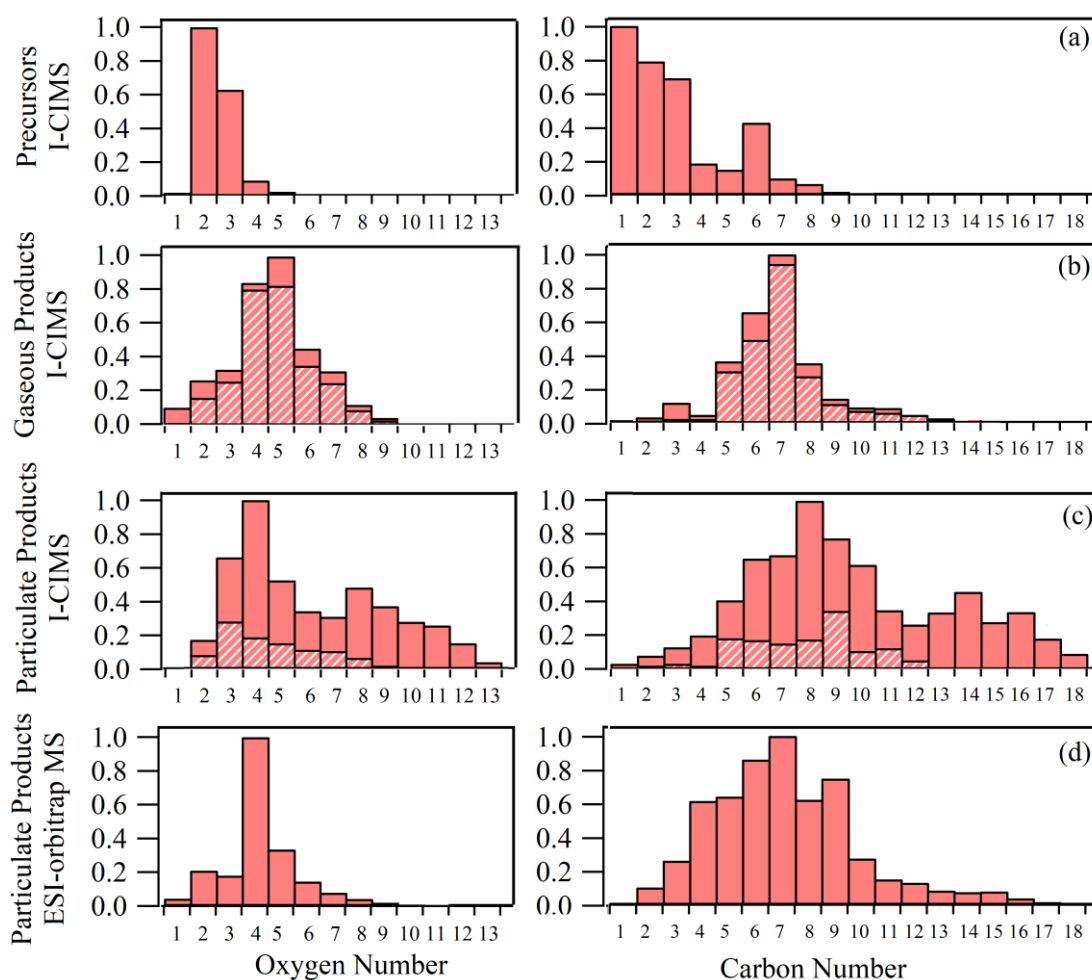
Figure 2. Oxygen and carbon atom number distributions of potential VOC precursors (a), gaseous products (b) and particulate products (c) measured by iodide-CIMS, as well as the particulate products measured by ESI-orbitrap MS (d) in a typical ozonolysis experiment (dynamic mode). Hatched bars indicate the fractions of organic formulas observed in both gas and particle phases by iodide-CIMS.